Cell Reports

Activation of the *Yersinia* type III secretion system induces large-scale spatial reorganization of chromosomal and virulence plasmid DNA

Graphical abstract

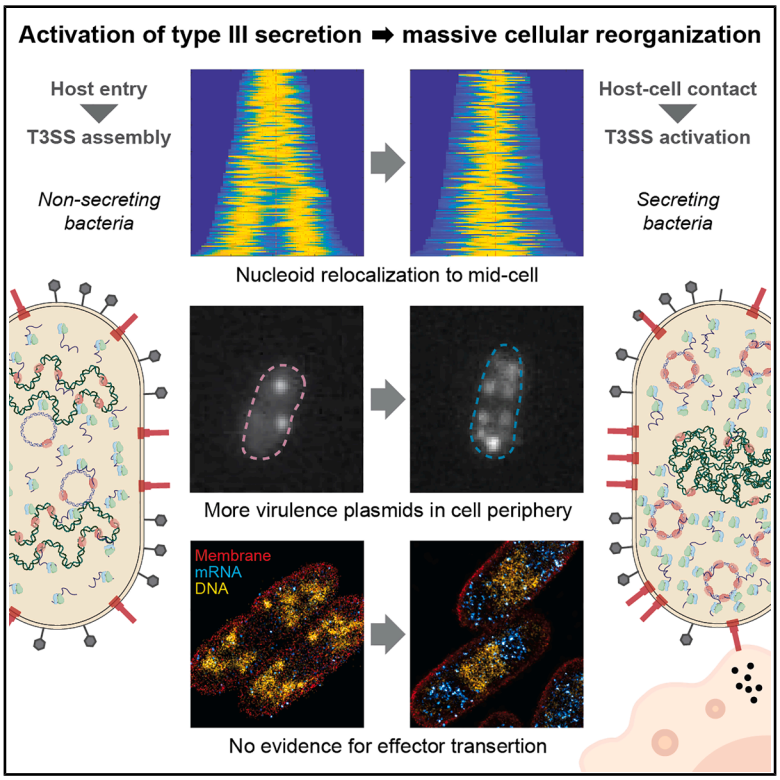

Authors

Francesca Ermoli, Christoph Spahn, Ismath Sadhir, Helge B. Bode, Andreas Diepold

Correspondence

andreas.diepold@kit.edu

In brief

Activation of the *Yersinia* type III secretion system triggers rapid, large-scale relocalization of both chromosomal and plasmid DNA. This spatial reorganization links secretion activity to growth inhibition, revealing a new connection between virulence and bacterial cell biology.

Highlights

- Upon T3SS activation, the *Yersinia* virulence plasmid localizes toward the cell periphery
- At the same time, chromosomal DNA shifts from quarter positions to mid-cell
- Effector mRNA localizes to the cytosol, indicating the effectors are not transerted
- T3SS-induced DNA reorganization provides insight into secretion-associated growth inhibition

Ermoli et al., 2025, Cell Reports *44*, 116592
December 23, 2025
https://doi.org/10.1016/j.celrep.2025.116592

CellPress

Cell Reports

CellPress
OPEN ACCESS

Report

Activation of the *Yersinia* type III secretion system induces large-scale spatial reorganization of chromosomal and virulence plasmid DNA

Francesca Ermoli,[1,8] Christoph Spahn,[2,3,8] Ismath Sadhir,[2,4] Helge B. Bode,[2,5,6] and Andreas Diepold[1,6,7,9,*]
[1]Department of Ecophysiology, Max Planck Institute for Terrestrial Microbiology, Marburg, Germany
[2]Department of Natural Products in Organismic Interactions, Max Planck Institute for Terrestrial Microbiology, Marburg, Germany
[3]Rudolf Virchow Center – Center for Integrative and Translational Bioimaging, Julius-Maximilians-University Würzburg, Würzburg, Germany
[4]Department Systems and Synthetic Microbiology, Max Planck Institute for Terrestrial Microbiology, Marburg, Germany
[5]Chemical Biology, Department of Chemistry, Philipps University of Marburg, Marburg, Germany
[6]Center for Synthetic Microbiology (SYNMIKRO), University of Marburg, Marburg, Germany
[7]Department of Applied Biology, Institute of Applied Biosciences, Karlsruhe Institute of Technology (KIT), Karlsruhe, Germany
[8]These authors contributed equally
[9]Lead contact
*Correspondence: andreas.diepold@kit.edu
https://doi.org/10.1016/j.celrep.2025.116592

SUMMARY

The type III secretion system (T3SS) is used by Gram-negative bacteria, including important pathogens, to manipulate eukaryotic cells by injecting effector proteins. Type III secretion and bacterial physiology are tightly interconnected. Notably, secreting cells undergo a secretion-associated growth inhibition in the T3SS model organisms *Yersinia*, *Salmonella*, and *Shigella*. In *Yersinia*, T3SS genes are encoded on the plasmid of *Yersinia* virulence (pYV), whose copy number increases upon induction of T3SS secretion. In this study, we characterize the link between T3SS activity and subcellular organization by localizing and quantifying pYV and chromosomal DNA in *Yersinia enterocolitica*. In secreting bacteria, pYV plasmids move toward the membrane and poles. We find no evidence for the transertion (coupled transcription, translation, and translocation) of a candidate effector, but we do find a striking relocation of chromosomal DNA to mid-cell. These findings reveal that T3SS activation coincides with large-scale reorganization of the bacterial nucleoid and plasmid DNA.

INTRODUCTION

The type III secretion system (T3SS) is used by many Gram-negative bacteria to manipulate the host during the establishment of an infection.[1–4] While it is a mediator of pathogenicity in many important pathogens, T3SS secretion can impose a metabolic burden on the bacteria and distinctly alter bacterial physiology. One of the most drastic effects is that T3SS-active cells display a severe growth retardation. This phenomenon, termed secretion-associated growth inhibition (SAGI), was the phenotype that initially led to the discovery of the T3SS, when researchers noted a strong growth inhibition specific to virulent *Yersinia* (now known to be equivalent to the presence of the T3SS) at 37°C (T3SS expression) in the absence of Ca^{2+} (T3SS activation).[5–10] While it has not been detected for all T3SSs, SAGI has been shown to occur in two other main T3SS model organisms besides *Yersinia*: *Salmonella enterica* and *Shigella flexneri*.[11–13] However, it is still unclear if SAGI is caused by the expression and export of the T3SS machinery and effectors or whether it is an actively regulated phenotype, as suggested by unaltered levels of key players of chromosome replication and segregation in secreting cells[14] and rapid reinitiation of cell growth and division when secretion is stopped.[15] To get insights into this intriguing connection between type III secretion and physiology, we investigated how the activation of the *Yersinia* T3SS affects the spatial organization of chromosomal and virulence plasmid DNA.

The T3SS, also called an injectisome, is a highly conserved multi-protein double-membrane-spanning nanomachine that enables the direct injection of effector proteins from the bacterial cytosol into the target host cell.[16] In the three *Yersinia* human pathogenic species, *Y. pestis*, *Y. enterocolitica*, and *Y. pseudotuberculosis*, the 70 kb plasmid of *Yersinia* virulence (pYV)[17] encodes for the T3SS machinery and the effectors, called *Yersinia* outer proteins (Yops). The *Yersinia* T3SS is essential for evading the immune system by preventing phagocytosis and the activation of the inflammatory cascade.[18] Expression and assembly of the T3SS machinery occur upon a temperature shift to the host temperature (37°C) via a complex regulatory cascade, ultimately inducing the synthesis of the main transcriptional activator of the system, VirF/LcrF

(reviewed in Volk et al.[19]). T3SS secretion is consequently activated by contact with the target host cell membrane, a condition efficiently mimicked *in vitro* by Ca^{2+} depletion in the culture medium.[20]

Activation of secretion leads to a strong upregulation of the production of effectors[21–24] but also a roughly 2-fold upregulation of the levels of injectisome components and consequently twice as many injectisomes per bacterium.[25] This is likely caused by a similarly increased number of pYV plasmids. In *Y. pseudotuberculosis*, the pYV plasmid copy number (PCN) increases from about one chromosome equivalent at 26°C to 1.5–2 upon host entry (37°C) and further to 3–4 over time.[26,27]

Next to the copy number, the localization of DNA can also have important consequences on cell physiology. Expression and assembly of the chromosome-encoded T3SS2 of *Vibrio parahaemolyticus* is likely mediated via transertion.[28,29] Transertion generates a dynamic link between the genomic locus and the inner membrane via coupling of transcription, translation, and insertion (or translocation) of proteins into (or across) the inner membrane. Particularly for low-abundant structures, such as the *V. parahaemolyticus* T3SS2, the spatial proximity of the gene and transcript to the site of insertion/translocation can enhance efficiency. Transertion can play a role in overall chromosome organization, particularly during phases of rapid growth. For example, the nucleoid of fast-growing *E. coli* cells is positioned near the membrane, and the disruption of transcription or translation leads to a rapid contraction of the bacterial nucleoid and loss of the putative link to the membrane.[29,30] Despite growing evidence for transertion, its role and effect on cell physiology are still unclear.

To investigate the effect of T3SS activation on bacterial cell biology, we compared key cellular parameters in secreting and non-secreting *Y. enterocolitica*. Strikingly, live-cell and super-resolution microscopy revealed a drastic reorganization of the bacterial DNA: activation of secretion led to a strong relocalization of the chromosomal DNA toward mid-cell within 30–60 min. By inhibiting the regular division at mid-cell, this profound reorganization of bacterial DNA upon activation of secretion could be a missing link in the SAGI of secreting bacteria. We further found that upon activation of the T3SS, the virulence plasmid not only increased in copy number but also relocalized toward the cell periphery. While effector mRNA was strongly upregulated under secreting conditions, it was not enriched at the bacterial membrane, arguing against the transertion of effectors. Taken together, the results show that activation of the T3SS leads to a previously unrecognized profound spatial reorganization of chromosomal and plasmid DNA associated with the SAGI of secreting bacteria.

RESULTS

pYV copy number is affected by temperature and T3SS activation

To investigate the influence of activation of the T3SS on pYV PCN, we quantified the PCN at 28°C and 37°C (host temperature) in a T3SS-deficient (Δ*sctD*) and a constitutively T3SS-active (Δ*sctW*) strain in this study. SctD is an essential inner-membrane structural component of the T3SS, while SctW is the main component of the gatekeeper complex, responsible for T3SS secretion inhibition prior to host-cell contact.[20,31] We will refer to these strains as non-secreting and secreting, unless specified otherwise.

Previous studies found that in *Y. pseudotuberculosis*, the copy number of the pYV virulence plasmid increases upon host entry (temperature shift to 37°C) and further upon activation of T3SS secretion.[26,32] To test this in *Y. enterocolitica*, we measured the ratio of the pYV copy number and the chromosomal copy number by qPCR, using the pYV-encoded T3SS transcription factor *virF*/*lcrF* and the chromosomally encoded *gyrB* genes as templates. Similar to the results in *Y. pseudotuberculosis*,[26] the pYV PCN increased from around 1 (28°C) to 2 at the host temperature (37°C, non-secreting) and further to 3–4 upon activation of secretion (37°C, secreting) (Figure 1A). To assess the cellular distribution of pYV plasmids and heterogeneity of the PCN under different conditions on a single-cell level, we inserted a $parS_{P1}$ sequence into a region of the pYV plasmid that is not required for T3SS function (the T3SS effector YopE) ($yopE_{1\text{-}138}$-$parS_{P1}$, Figures S1A and S1B). Expression of an mScarlet-I fusion to the corresponding ParB protein, mScarlet-I-$ParB_{P1}$, from an inducible plasmid led to the detection of fluorescent foci. We chose this approach over using the native ParB/*parS* system so as not to interfere with pYV replication and segregation. Correct pYV segregation in the $yopE_{1\text{-}138}$-$parS_{P1}$ strain expressing mScarlet-I-$ParB_{P1}$ was confirmed by a consistently high number of bacteria with EGFP-SctQ foci, whose presence depends on the presence of the pYV plasmid (Table S1). The functionality and stability of the mutants and the specificity of the mScarlet-I-$ParB_{P1}$-$parS_{P1}$ spot formation were confirmed (Figures S1C–S1E). Single-cell quantification of $ParB_{P1}$ foci yielded results highly comparable with the qPCR data (Figure S2). It confirmed the effect of both temperature and T3SS activation on the PCN and highlighted a considerable heterogeneity in the pYV copy number (Figure 1B).

T3SS activation induces a relocalization of the pYV plasmid toward the membrane

Next, we assessed the localization of the pYV plasmid in secreting and non-secreting bacteria. First, we determined the localization along the width of the cell by measuring the distance of the plasmid from the longitudinal centerline. The distribution of the T3SS component SctQ (EGFP-SctQ)[33] was taken as a control for membrane localization. In T3SS-active cells, the pYV plasmids localized significantly closer to the membrane than in non-secreting cells (Figure 1C). As spot distributions were symmetric, statistics were performed on the absolute values. Different from the PCN, which increased upon both temperature shift and T3SS triggering (Figure 1), pYV plasmid relocalization was only observed upon induction of secretion (Figure 1C). This was not a consequence of PCN increase, as T3SS-active cells with one or two pYVs showed a similar shift of pYV localization from the centerline toward the membrane compared to the other conditions tested (Figure 1D).

Next, we quantified the relative position of the pYV plasmid along the longitudinal axis (central vs. polar localization). In secreting bacteria, the virulence plasmids were strongly shifted from the center toward the poles of the bacteria. Like in the previous experiment, we also compared cells with one or two foci in

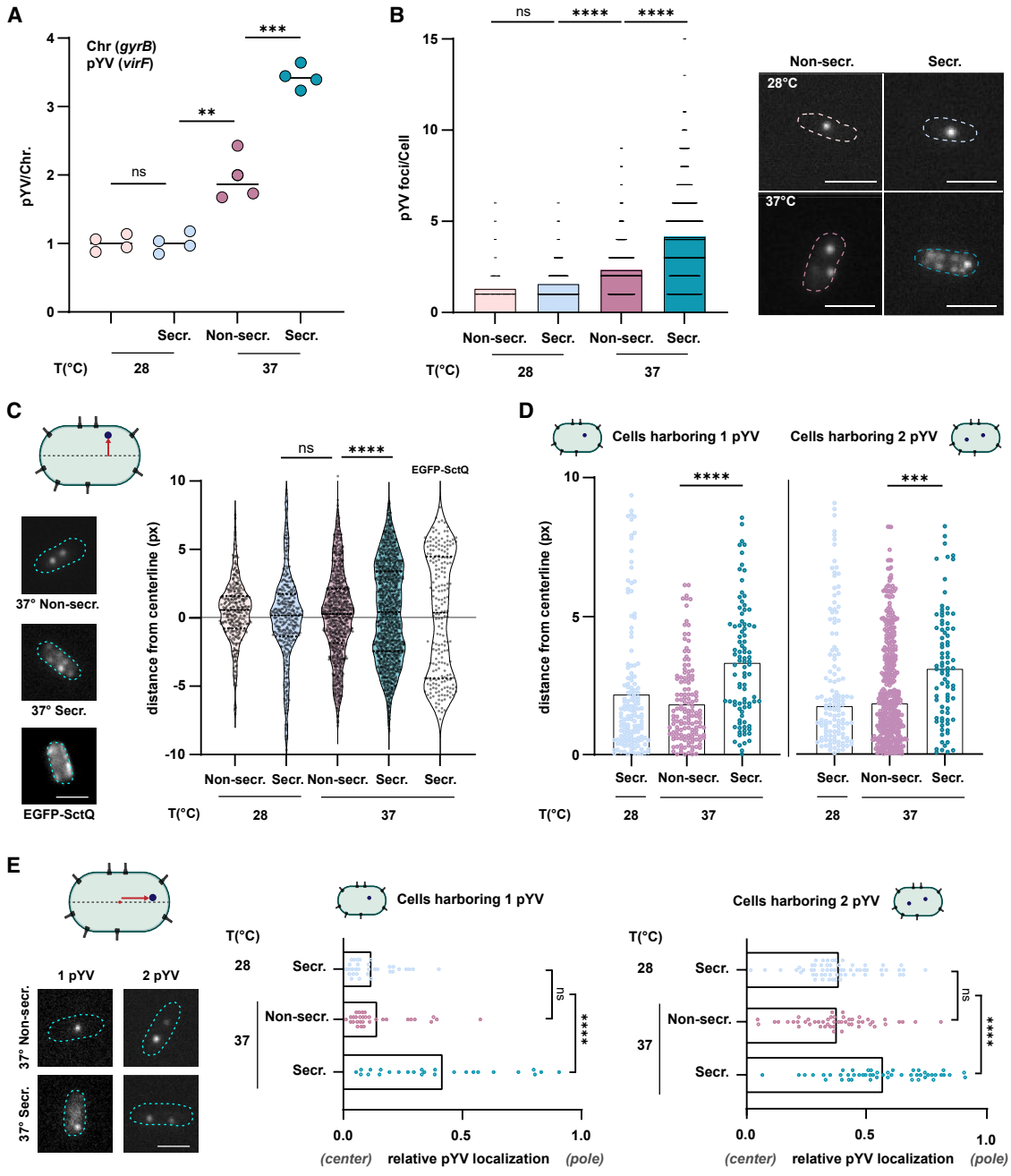

Figure 1. Activation of the T3SS leads to increased pYV copy number and plasmid relocalization toward the membrane and poles

(A) Plasmid copy number expressed as pYV (*virF*)/number of chromosome equivalents (*gyrB*) in non-secreting (non-secr.; Δ*sctD*) and secreting (secr.; Δ*sctW*) bacteria at 28°C and 37°C, as determined by qPCR. $n = 4$.

(B) Quantification of pYV ($yopE_{1\text{-}138}$-$parS_{P1}$) spots per bacterium, visualized by fluorescence microscopy in strains expressing mScarlet-I-$ParB_{P1}$ under different conditions as in (A). Sample micrographs are depicted on the right; scale bar, 2 μm. The correlation between the results from (A) and (B) is shown in Figure S2.

(C) Single-cell pYV plasmid localization ($yopE_{1\text{-}138}$-$parS_{P1}$) measured as distance from the centerline (px) in the indicated conditions. EGFP-SctQ was used as a control for membrane localization. Left, representative fluorescence micrographs for the three indicated strains.

(D) As in (C) but for cells displaying one spot (left) or two spots (right).

(E) Single-cell pYV plasmid localization along the longitudinal axis for cells displaying one (left) or two (right) spots. To account for differences in cell length, the relative localization of plasmids is displayed: 0 = center of cell and 1 = cell pole. Left, representative fluorescence micrographs for the indicated strains.

In all experiments, measurements were performed 150 min after the indicated cultures were shifted to 37°C (and at the same time for the cultures continuously incubated at 28°C); see the STAR Methods for details; $n = 3$.

the different conditions and found that the relocalization of pYV plasmids toward the poles was independent of the increase in PCN (Figure 1E).

Synthesis and secretion of the effector YopM are uncoupled

It has been speculated that T3SS-harboring bacteria may benefit from using transertion during injectisome assembly[29] or substrate secretion. Transertion couples co-transcriptional translation and protein insertion at the site of action or export to optimize synthesis efficiency.[28,34,35] As this process requires the presence of the target gene at the site of protein insertion, we wondered whether the observed relocalization of pYV plasmids under secreting conditions is caused by transertion. As transertion requires mRNA to be localized near the membrane, we investigated the localization of the mRNA of the T3SS effector YopM using RNA fluorescence *in situ* hybridization (RNA-FISH). YopM is a particular candidate for cotranslational secretion—while most *Yersinia* T3SS effectors have cognate chaperones that keep their effectors in a cytosolic secretion-competent state, YopM does not have a known chaperone.[36,37] To visualize YopM transcripts with bacterial DNA and membrane, we performed super-resolution imaging using single-molecule localization microscopy (SMLM). We used DNA point accumulation for imaging in nanoscale topography (DNA-PAINT) coupled with RNA-FISH (super-resolution single-molecule RNA FISH [sr-smRNA-FISH]) (Figure 2A), where transient hybridization of a target complementary strand (docking strand) and a short dye-labeled oligonucleotide (imager strand) enables multiplexing and high accuracy during super-resolution imaging.[38] Nearest-neighbor analysis (NeNA)[39] yielded a localization precision of 10–11 nm (resolution of ~25 nm). We found a strong signal in the positive control (eubacteria-specific rRNA probe EUB338) and no signal in the negative control (no FISH probe) (Figure S3). DNA and membranes were visualized by conventional PAINT,[40] and all channels were overlaid to visualize the spatial context of *yopM* mRNA, the nucleoid, and the cell envelope (Figure 2B). *yopM* mRNA abundance strongly increased in secreting conditions, with transcripts being excluded from the nucleoid area (Figure 2B, yellow). However, we did not observe a specific enrichment at the cell membrane, but we did see an apparently higher density at the cell poles and between the sister chromosomes (Figures 2B and S4). This observation is independent of cells having one or two separated nucleoids (Figure S5). To get a more quantitative assessment of mRNA distribution, we determined its average distribution relative to the nucleoid (Figures 2C and S5). Intensity measurements along the bacterial long axis support the visual assessment, revealing a pole-shifted distribution of the *yopM* mRNA signal relative to the nucleoid (Figure S6). 3D DNA-PAINT imaging further showed that mRNA is distributed throughout the cytosol, also in high-density regions at the cell poles, ruling out artifacts by 2D projection of 3D distributions (Figure S7). Taken together, our observations argue against transertion as a strategy used for YopM synthesis and secretion. We further quantified transcript abundance by counting localization clusters in sr-smRNA-FISH measurements using density-based spatial clustering of applications with noise (DBSCAN)[41] (Figure S8). Here, the number of transcripts under secreting conditions correlated with cell size (Figure 2D). Under non-secreting conditions, only slightly more transcripts were detected than in the negative control (2.4 ± 2.8 vs. 1.2 ± 1.1 clusters, SD, n = 176 and 33 cells for non-secreting cells and the control, respectively). 150 min after induction of secretion, we observed an ~13-fold increase in transcript abundance, with a high variability between single cells (31 ± 13 clusters, SD, n = 531 cells from 4 replicates) (Figure 2E), while the mean values of individual replicates were highly reproducible (31 ± 4 clusters, SD). Similar trends were seen for the cluster density (number of clusters per μm^2 cell area) (Figure S9). At the subcellular level, the cluster density under secreting conditions appears to be higher at the poles, where we also observed a higher abundance of ribosomes, in accordance with previous results[42] (Figure 2F). We thus conclude that the *yopM* mRNA freely diffuses in the cytosol and gets captured at ribosome-dense regions by uncoupled translation.

T3SS activation alters chromosomal DNA organization

Upon activation of T3SS secretion, *Yersinia* cells display cell growth retardation[5,15] and cell elongation.[43] Measuring cellular dimensions in non-secreting and secreting cells revealed a 12% increase in mean cell length from 2.70 to 3.03 μm and a corresponding larger cell area of secreting bacteria (Figures 3A–3C). As cell elongation and growth retardation could be explained by a defect in chromosome replication or segregation, we compared the DNA distribution in the previously tested conditions by DAPI staining. Secreting and non-secreting cells showed a drastically different DNA organization. The majority of non-secreting cells displayed two intensity spots at quarter positions, comparable to wild-type cells grown at 28°C (Figure 3D), while secreting cells showed the highest fluorescence intensity at mid-cell, independent of their cell length (Figure 3D). The altered DNA organization of secreting bacteria was still present, albeit slightly reduced, in *Y. enterocolitica* lacking the main virulence effectors YopH, -O, -P, -E, -M, and -T (Figure S10), indicating that the strong expression of these genes and other T3SS components might contribute to this phenotype.

Secretion leads to increased PCN and nucleoid rearrangement within 15–60 min

To temporally resolve the cellular rearrangements following T3SS activation, secretion was induced by Ca^{2+} chelation in a natively Ca^{2+}-responsive *Y. enterocolitica* strain, and the pYV copy number and localization, cell length, and DNA organization were assessed as previously described (Figures 1B–1E and 3) at the time of induction (T_0) and 15 (T_{15}), 30 (T_{30}), or 60 (T_{60}) min post-induction (Figure 4A). The pYV PCN gradually increased from the first time point tested, from an average value of 2.4 ± 1.2 at T_0 to a PCN of 3.7 ± 2.0 at T_{60}. As the full replication of the 70 kb pYV takes a few minutes (2 min at a replication speed of 600 bp/s), we assume that the initiation of pYV replication is rapidly initiated upon activation of secretion.

Plasmids showed a more peripheral localization at T_{60} than at T_0. As for the pYV PCN, plasmid localization was significantly shifted from the first time point tested (T_{15}) compared to T_0 (Figure 4B). Importantly, a clear transition from a bipolar quarter-cell DNA distribution, typical of replicating and dividing cells, to a mid-cell DNA localization occurred upon the activation of secretion (Figure 4C). While our measurements indicate that this effect

CellPress
OPEN ACCESS

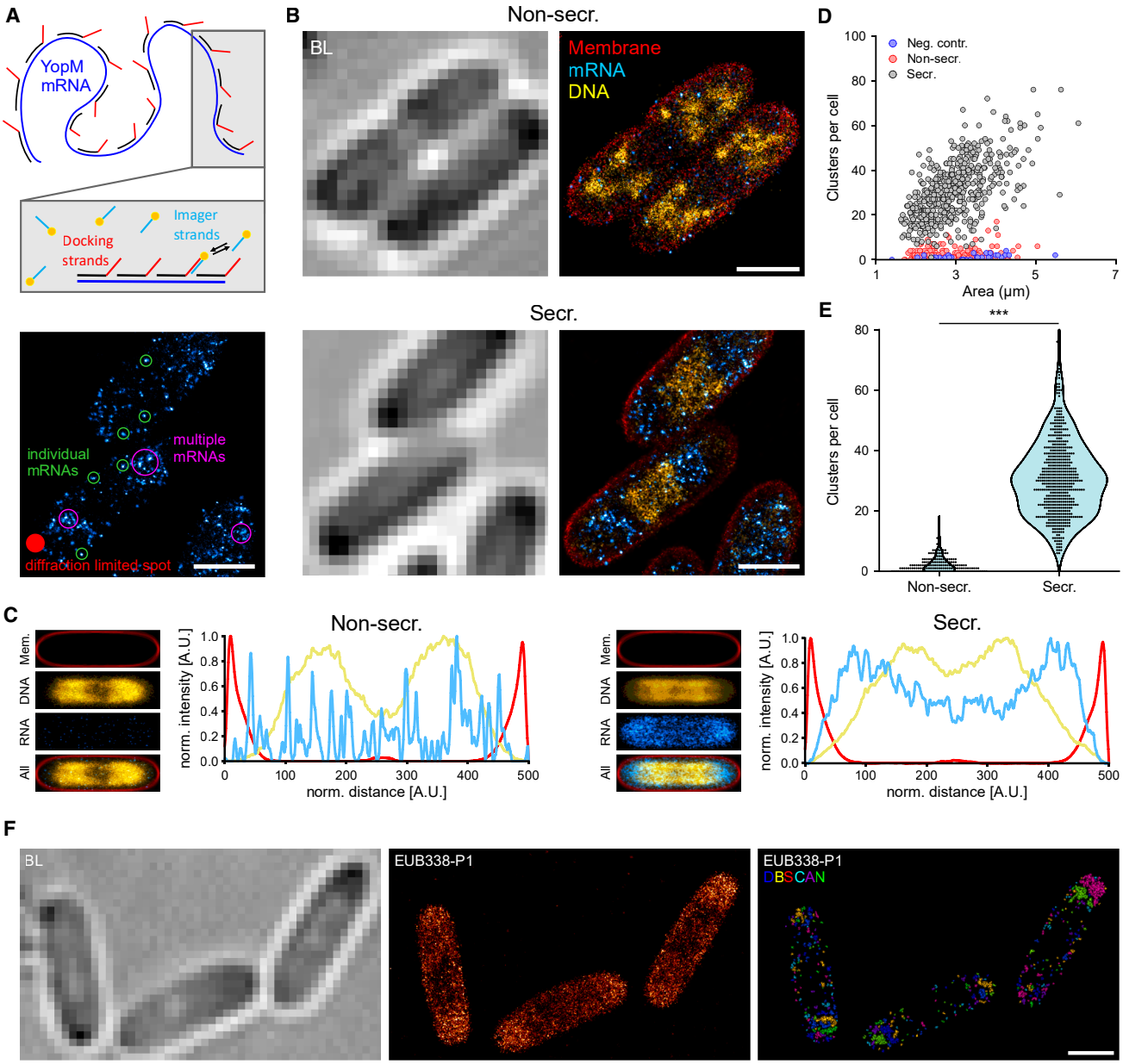

Figure 2. YopM mRNA localizes to the cytosol, but not to the membrane, upon T3SS induction

(A) Super-resolution single-molecule RNA fluorescence *in situ* hybridization (sr-smRNA-FISH) scheme (top). The mRNA (*yopM*, blue) is targeted by short RNA-FISH oligos containing a non-hybridizing docking sequence (docking strand). RNA-FISH label positions are read out via DNA-PAINT using the transient hybridization of ATTO655-labeled imager strands. The resulting super-resolved images report on mRNA localization and clustering (bottom).

(B) Representative super-resolution images of non-secreting and secreting *Y. enterocolitica* (non-secr./secr.) fixed with formaldehyde. The membrane (red) and DNA (yellow) were visualized using PAINT and mRNA (cyan hot) using DNA-PAINT. See Figures S4 and S5 for a larger gallery of images, including secreting cells with two nucleoid foci.

(C) Intensity distribution along the bacterial long axis in population averages of non-secreting and secreting bacteria. Colors are the same as those in (B). Separated nucleoids under non-secreting conditions merge and reposition toward the center under secreting conditions. Population averages and line plots reveal a separation between *yopM* mRNA and the nucleoid, with *yopM* mRNA being localized toward the cell poles. Note that under non-secreting conditions, only a little mRNA signal is observed. See Figure S6 for details.

(D) Correlation between detected sr-smRNA-FISH clusters and cell size. $n_{replicates}$ = 3, 4, and 1 and n_{cells} = 176, 531, and 33 for non-secreting cells, secreting cells, and the negative control (no FISH probes), respectively.

(E) Quantification of sr-smRNA-FISH clusters under the indicated conditions (*n* as in C). Statistical analysis was performed using a Mann-Whitney U test.

(F) sr-smRNA-FISH of rRNA. rRNA was visualized via DNA-PAINT using a docking-strand-containing EUB338 probe (EUB338-P1) targeting 16S rRNA (middle). Cluster analysis using the DBSCAN algorithm shows large rRNA clusters at the cell poles. Clusters are individually colored by cluster index. Scale bars, 1 µm.

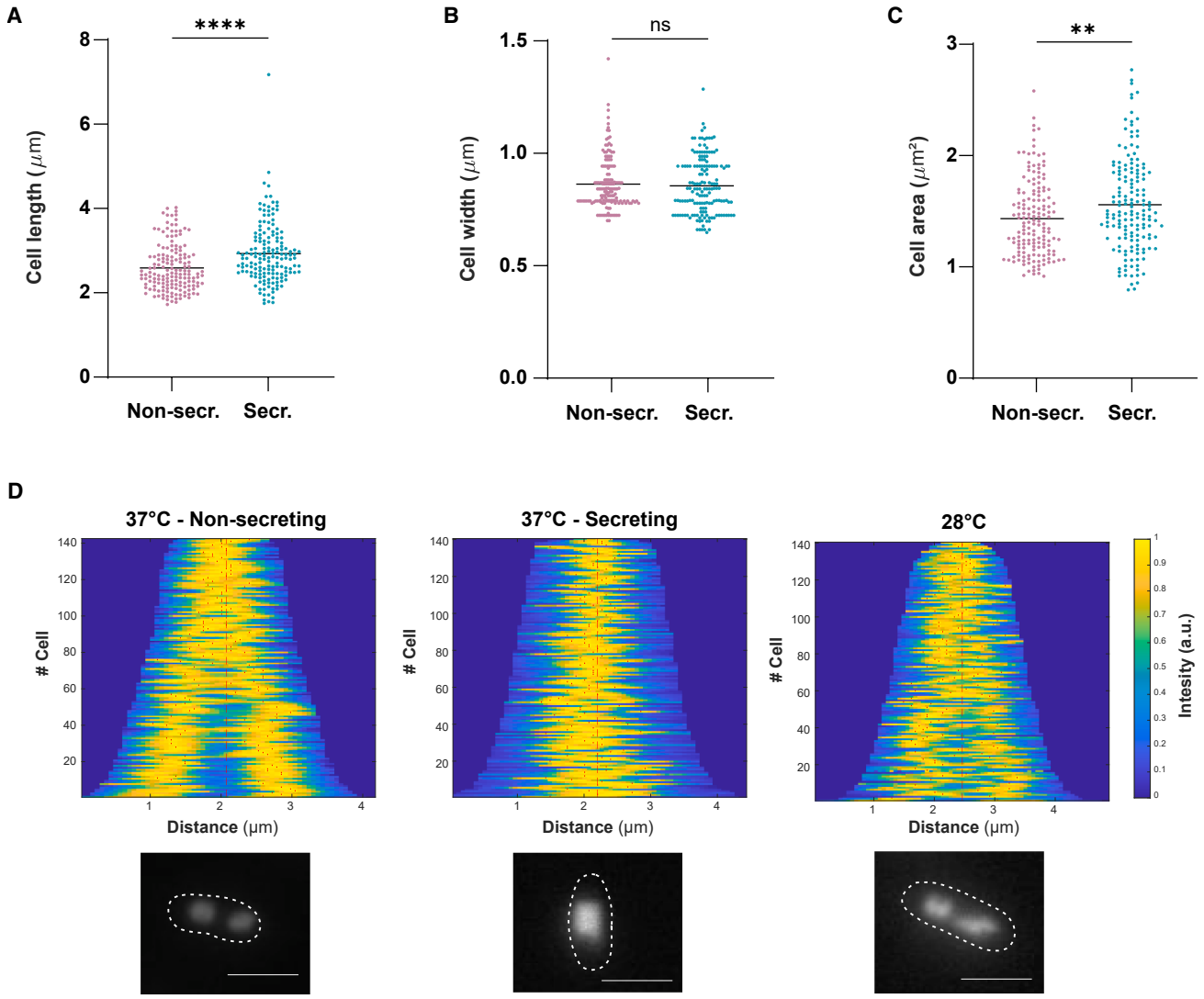

Figure 3. Cell length and DNA organization are affected by T3SS activation

(A–C) Cell length, width, and area measured in non-secreting (non-secr.; 37°C, Δ*sctD*) and secreting (secr.; 37°C, Δ*sctW*) bacteria, 150 min after induction of T3SS expression by temperature shift to 37°C.

(D) Chromosome organization of wild-type bacteria at 37°C in non-secreting (Δ*sctD*) and secreting (Δ*sctW*) bacteria and 28°C in the wild type. In the demographs, cells are sorted according to cell length, and DAPI signals are shown according to the intensity scale. Small red points represent intensity peaks. Bottom, representative fluorescence microscopy images of cells stained with DAPI. Scale bar, 2 μm.

n = 3 for (A)–(D).

is partly caused by bacteria completing their division within this time range (Figure S11), relocalization of the chromatin may also contribute to this effect. After this rapid reorganization, further changes of pYV and chromosome organization are more subtle, as shown by similar phenotypes observed for 60 and 150 min time points (Figures 1C and 4B).

DISCUSSION

The T3SS is an essential virulence factor for a broad range of Gram-negative bacteria. In *Yersinia* and other pathogens, secreting cells display a growth impairment (SAGI).[5,44] Despite the striking phenotype, the nature of the link between T3SS secretion and bacterial growth is highly debated.[45–47] The energy demand of assembling and operating the T3SS has been proposed as a possible cause of the growth suppression.[48–50] Early work in *Y. pestis* suggested that T3SS activation reduced the adenylate energy charge, defined as ([ATP] + ½[ADP])/([ATP] + [ADP] + [AMP]), but this effect was later shown to be the secondary rather than the primary cause of SAGI.[51] Consistently, the growth phenotype occurs in both minimal and rich media. Moreover, bacteria can still grow while assembling and running energetically demanding systems, such as flagella—larger structures that continuously dissipate the proton-motive force—or T6SSs, which

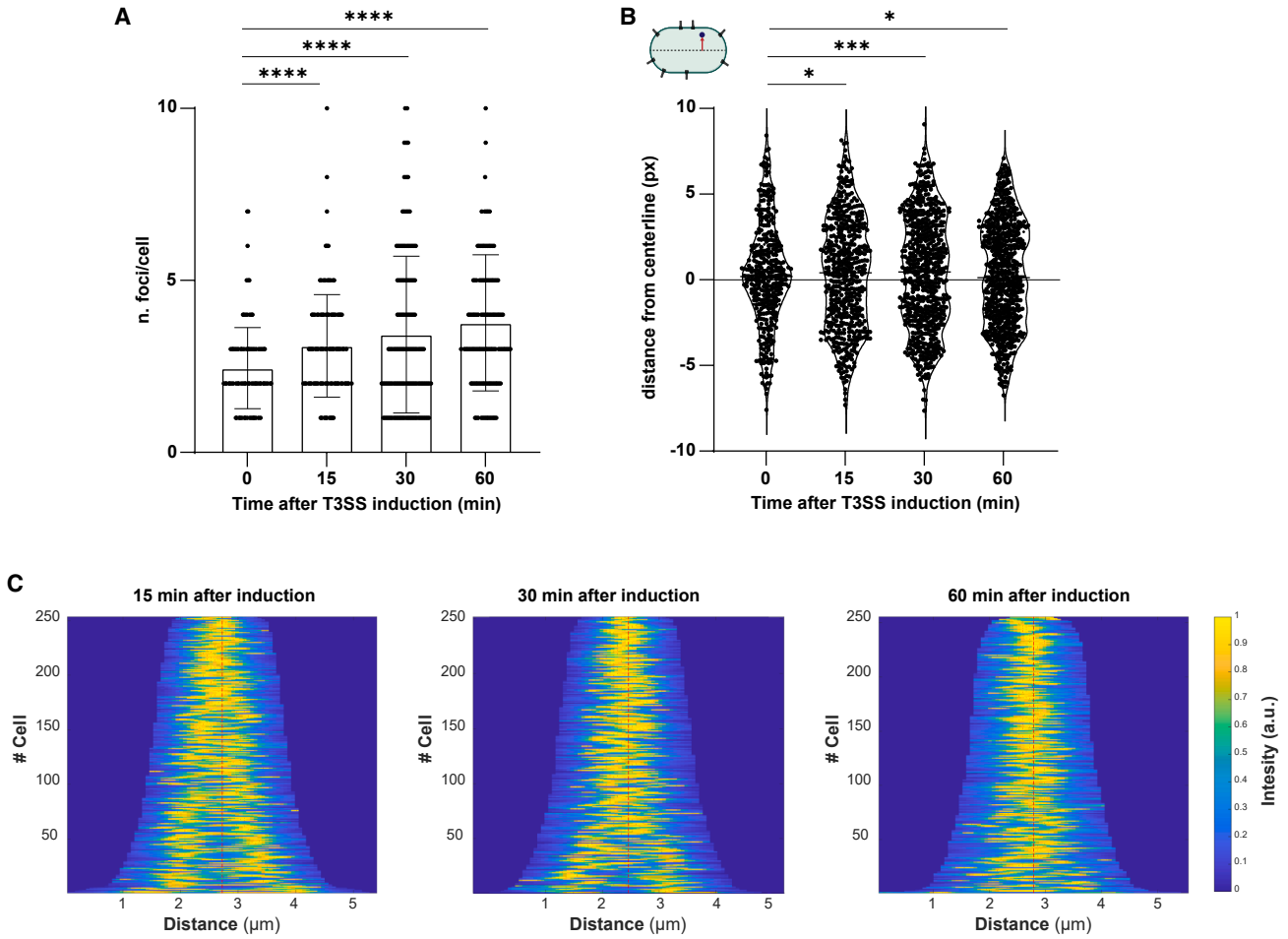

Figure 4. Kinetics of cellular rearrangement upon T3SS induction

(A) Quantification of pYV (*yopE*$_{1\text{-}138}$-*parS*$_{P1}$) spots per bacterium, visualized by fluorescence microscopy before and 15, 30, or 60 min after T3SS induction by Ca^{2+} chelation at 37°C. Each dot represents a single bacterium.

(B) Single-cell pYV plasmid localization (*yopE*$_{1\text{-}138}$-*parS*$_{P1}$) measured as distance from the centerline (px) in the conditions described in (A).

In (A) and (B), each dot represents a single localization.

(C) Cell length and chromosome organization of *Yersinia* cells in the conditions described in (A). In the demographs, cells are sorted according to cell length, and DAPI signals are shown according to the intensity scale. Small red points represent intensity peaks.

$n = 3$ for (A)–(C).

require large bursts of energy for firing.[52,53] More directly, our group demonstrated that *Y. enterocolitica* strains lacking all six major virulence effectors,[54] which normally account for more than half of exported proteins under secreting conditions, show a SAGI only slightly reduced.[15] This argues against energy expenditure as the main cause. In agreement, the adenylate energy charge of secreting bacteria remains unchanged.[15] Since ATP synthesis relies on the proton motive force (PMF), any substantial PMF depletion would directly lower ATP levels, indirectly suggesting that secretion does not significantly impair the PMF either. Thus, the molecular basis and potential advantage of the SAGI remain unresolved.

To shed light on this mechanism, we investigated key cellular parameters of secreting and non-secreting *Y. enterocolitica* at the single-cell level. The proposed role of SAGI as a strategy to preserve the energetic status of the cell is based on the observation that T3SS machinery components and especially the effectors are significantly upregulated upon secretion induction (reviewed in Volk et al.[19]). In *Y. pseudotuberculosis*, it was shown that during secretion, this upregulation correlates with an increase in the pYV PCN,[26,27] a finely regulated phenotype present in similar form for the *S. flexneri* pINV virulence plasmid.[55] We confirmed and further characterized this phenotype in single *Y. enterocolitica* cells using a ParB/*parS*-based pYV labeling system (based on Sadhir and Murray[56]) (Figure S1), revealing the large heterogeneity of PCNs in non-secreting and secreting bacteria, with secreting cells containing one to more than ten pYVs (Figure 1B). As previously observed for *Y. pseudotuberculosis*,[26] the pYV PCN was increased by both a temperature shift to 37°C (equivalent to host entry) and activation of the T3SS, leading to two sequential PCN upregulation steps (Figures 1A and 1B). We observed about four pYV foci in secreting *Y. enterocolitica*, similar

to and slightly below the numbers in an earlier[26] and a recent[55] study *in Y. pseudotuberculosis*, respectively. Surprisingly, we found that virulence plasmids relocalize toward the membrane and the bacterial poles in secreting bacteria independent of the PCN (Figures 1C–1E). A possible reason for the relocation toward the membrane is transertion,[28] which was recently found to mediate T3SS2 assembly in *V. parahaemolyticus*.[29] The transcriptional activator of this T3SS, which, unusually, is a transmembrane protein, captures the T3SS gene locus and therefore leads to the transcription of T3SS components and effectors at the membrane.[29] Since in *Y. enterocolitica*, T3SS genes are encoded on the extra-chromosomal pYV plasmid, transertion would lead to a membrane localization of the pYV when the T3SS is assembled (shifts to 37°) or upon activation of secretion, when large amounts of effectors are synthesized and exported.[57] While the majority of *Yersinia* T3SS effectors have dedicated chaperones with a wide range of roles, including keeping their cognate effectors in a secretion-competent state, and effector-chaperone complexes are readily detected in the bacterial cytosol,[58] some effectors do not have chaperones, which makes them prime candidates for transertion. We therefore investigated whether transertion is involved in the secretion of YopM, a T3SS effector protein that belongs to this subgroup.[36,37] Investigating the subcellular localization of *yopM* transcripts using super-resolution microscopy revealed a strong upregulation under secreting conditions (Figure 3). *yopM* mRNA is excluded from the nucleoid but does not show a specific membrane enrichment (Figures 2A, 2C, S5, and S6). We thus conclude that transertion is not required for the secretion of this type of effector protein.

An alternative explanation for the strong movement of pYV plasmids toward the membrane and bacterial poles is that increased T3SS gene expression during secretion acts as a driving force for the separation of pYV plasmids and transcription-translation machinery from the nucleoid region.[59,60] It has been recently shown that enhanced extra-chromosomal gene expression induces ribosome accumulation at the synthesis site, leading to DNA compaction and defects in chromosome segregation.[42] Like *E. coli*, *Yersinia* does not harbor any known active ParABS system to assist with chromosome segregation, leaving the driving forces of this process open. To determine if increased pYV gene expression during secretion is accompanied by a relocalization of chromosomal DNA in *Yersinia*, we localized DNA in T3SS-active cells with high resolution using PAINT.[40] Live-cell imaging of DAPI-stained DNA showed a markedly altered DNA distribution upon secretion activation, changing from a largely bifocal one-quarter/three-quarter positioning to a unifocal central positioning, independently of the cell size (Figure 3D). This can be at least partly explained by bacteria finishing their cell division during this time (Figure S11). If and to what degree nucleoid relocalization in non-dividing bacteria contributes to the effect remains open.

Interestingly, pYV PCN and localization significantly changed already after 15 min of T3SS induction, concomitantly with chromosome reorganization (Figure 5). A fast response of the pYV plasmid and consequent chromosome rearrangement would be compatible with reorganizations in the transcription/translation machinery. Large molecular assemblies, such as highly transcribed genes, were found to localize to the nucleoid surface to maximize entropy.[61,62] Upon secretion induction, genes on the pYV, especially the effectors, get highly transcribed, likely forming large molecular assemblies that segregate from the nucleoid region, similar to highly transcribed genes from the nucleoid core. This is in agreement with a study by Martin et al.,[63] in which the relocation of *rrn* operons from the chromosome to a plasmid led to the formation of RNA polymerase assemblies at the cell poles. Typically, low-copy-number plasmids, such as the pYV, are linked to the nucleoid via the interaction of ParA and ParB and segregate together with the nucleoid.[64,65] Our results, however, indicate a spatial separation of pYVs from the nucleoid during secreting conditions, as pYVs localize toward the membrane and cell poles (Figures 1C and 4B), while the nucleoid repositions toward the cell center (Figures 3D and 4C). A possible explanation could be that pYVs dissociate from the nucleoid due to the high transcriptional activity on pYV-encoded genes under secreting conditions. RNA polymerase is known to remove roadblocks on DNA,[66] and high transcriptional activity could thus break ParA/ParB-mediated linkage of the pYV to the chromosome. The highly transcribed pYV is further a large molecular assembly that could relocate within the cell due to phase separation, as observed for other molecular assemblies, such as the previously mentioned RNA polymerase clusters[62] or polysomes.[67] In addition to pYV relocalization, effector mRNAs are highly transcribed,[68] as T3SS effectors account for a large fraction of the proteome under secreting conditions. Such mRNAs are thus expected to be localized in ribosome-dense regions of the cell.[41] This is in agreement with our super-resolution images, which show an enrichment of *yopM* mRNA and ribosomes at the polar cell regions. Consequently, the increased concentration of molecular crowders could then drive chromosome compaction, as demonstrated by rapid nucleoid compaction by increasing molecular crowding in *E. coli* upon an osmotic shock.[69] This hypothesis is supported by our observation that secreting bacteria lacking effectors show a less pronounced relocalization of the chromosomal DNA to the cell center (Figure S10), possibly due to the reduced transcript abundance. While the findings above support the hypothesis that strong transcription and translation cause the segregation of the virulence plasmid from the nucleoid and its subsequent relocation, they do not rule out other explanations, such as the possibility that nucleoid compaction in secreting bacteria by unknown means would disrupt the nucleoid association of the pYV plasmid. Intriguingly, irrespective of the cause, the resulting central localization of chromosomal DNA likely prevents cell division by nucleoid occlusion,[70,71] which may be a causal or contributing factor for the SAGI.[72,73]

Taken together, our data highlight the extent and nature of DNA rearrangement in secreting bacteria and provide a possible reason for the SAGI (Figure 5), which—more than six decades after the discovery of the T3SS through this phenotype—is still a conundrum. Further single-cell studies of these events in other bacteria may help to discern the conservation of this striking phenotype and potential species-specific adaptations.

Limitations of the study

The experiments in this study were performed with bacteria harboring a constitutively active or inactive T3SS and wild-type bacteria whose T3SS was activated by low extracellular

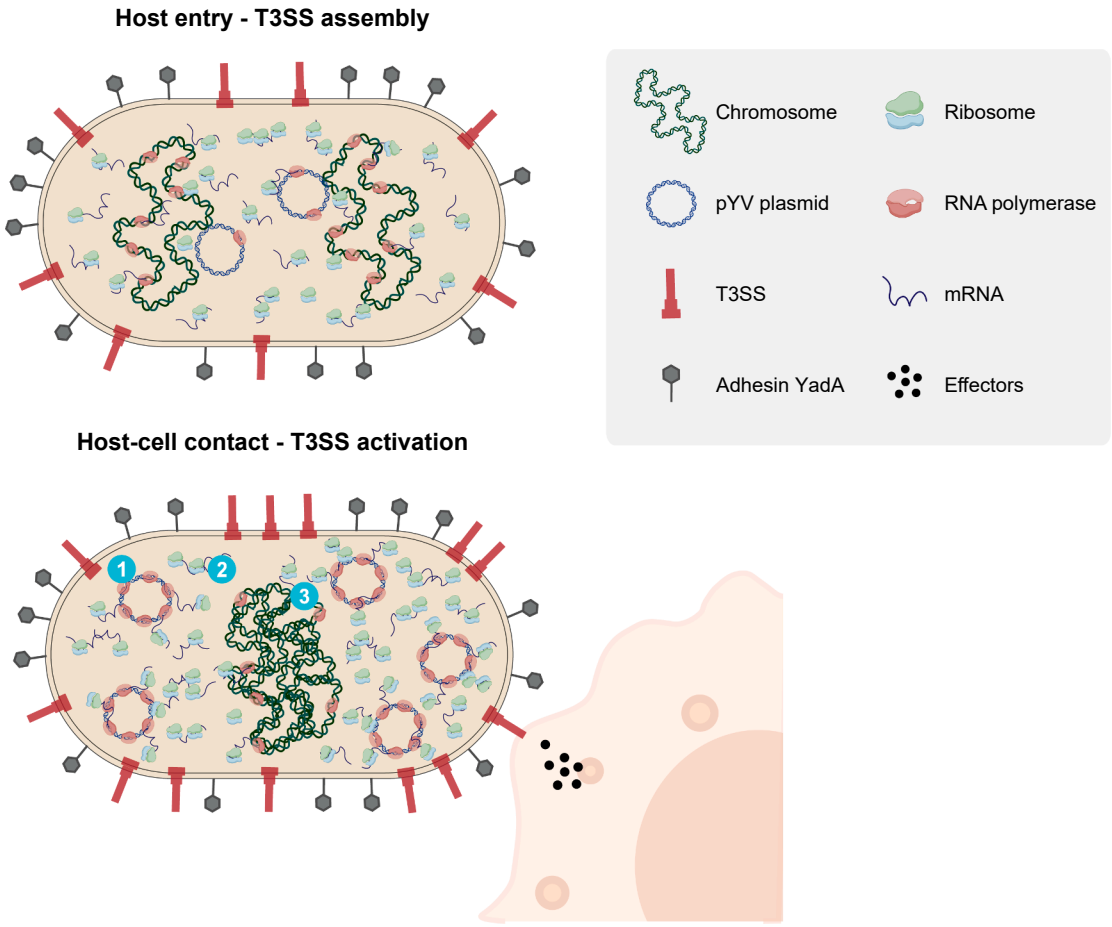

Figure 5. Influence of T3SS secretion on bacterial cell architecture

Yersinia relies on the adhesion protein YadA (depicted in gray on the bacterial surface) and effector secretion by the T3SS (depicted in red on the bacterial surface) to colonize the host by fighting the host's immune system. Upon host entry, in the absence of host-cell contact (top), the T3SS machinery is assembled, but secretion remains inactive.[74] At this stage, the pYV PCN (circular DNA depicted in blue) is, on average, about 1–2 per number of chromosomal equivalents. Host-cell contact and T3SS activation (bottom) lead to increased assembly of T3SS and strong upregulation of T3SS effector expression.[20,75] Simultaneously, the pYV PCN increases, and the plasmids are excluded from the nucleoid, possibly due to the upregulation of T3SS genes (① in figure). Under these conditions, effector transcripts (depicted as a single filament in blue) accumulate in the polar regions but without specific enrichment at the membrane. Increased expression of T3SS genes induces redistribution of the transcription and translation machinery (ribosomes depicted in light blue and green) away from the chromosome (depicted in green as a double-helix string) (②), possibly preventing or reversing chromosome segregation (③),[42] which might then block cell division. Parts of the scheme were generated using BioRender.

calcium concentrations. This enabled us to investigate secreting and non-secreting bacteria in a clearly defined manner. However, this approach might not be fully representative of the natural infection cycle, in which the T3SS is activated by target cell contact. Future experiments in infection models would be required to confirm the observed phenotype in more native settings. Another limitation is the focus on YopM, a promising candidate for a transerted effector protein, given its lack of a cognate chaperone. Our observation that YopM expression and secretion likely do not involve transertion does not generally rule out a role of transertion in the expression and localization of other effectors or T3SS components. Applying the sr-smRNA-FISH approach established in this study to other T3SS components may provide a more holistic view of T3SS and virulence factor expression dynamics. Finally, two important questions regarding the mechanism of SAGI remain open: (1) at which time point does SAGI interfere with cell division and (2) is the observed reduction of cell division a direct consequence of the striking relocalization of chromosomal DNA to mid-cell? These questions might be tackled using microfluidic devices that allow us to directly study the transition from non-secreting to secreting conditions at high temporal resolution.

RESOURCE AVAILABILITY

Lead contact

Requests for further information, resources, and reagents should be directed to the lead contact, Andreas Diepold (andreas.diepold@kit.edu).

Materials availability

Requests for resources and reagents should be directed to the lead contact.

Data and code availability

The model used for the segmentation of individual *Y. enterocolitica* cells for data analysis and demograph generation is deposited on Zenodo within the DeepBacs repository under the accession code: 11105050. This study does not contain original code. Additional information required for further analysis or reanalysis is available through the lead contact upon reasonable request.

ACKNOWLEDGMENTS

This work was supported by the Max Planck Society. F.E. acknowledges funding by the International Max Planck Research School Principles of Microbial Life. C.S. acknowledges funding by the State of Bavaria via the Distinguished Professorship Program 3.1-3122.05-008/014 P000122427. We thank all members of the Diepold lab for helpful discussions.

AUTHOR CONTRIBUTIONS

F.E., C.S., and A.D. were involved in the conception and design of the study. F.E. performed the majority of the molecular biology experiments. C.S. and F.E. performed the super-resolution studies and analyzed the microscopy data. I.S. provided resources and participated in the interpretation. H.B.B. provided supervision and resources. F.E., C.S., and A.D. wrote the manuscript with the support of all authors.

DECLARATION OF INTERESTS

The authors declare no competing interests.

STAR★METHODS

Detailed methods are provided in the online version of this paper and include the following:

- KEY RESOURCES TABLE
- EXPERIMENTAL MODEL AND STUDY PARTICIPANT DETAILS
- METHOD DETAILS
  - Bacterial strain generation and genetic constructs
  - Bacterial cultivation, secretion assay, and protein detection
  - Fluorescence microscopy
  - Quantification and localization of fluorescent pYV foci
  - mRNA fluorescence *in situ* hybridization
  - Single-molecule imaging
  - Counting of mRNA clusters
  - Measurement of intensity profiles in super-resolved population average images
  - qPCR
- QUANTIFICATION AND STATISTICAL ANALYSIS

SUPPLEMENTAL INFORMATION

Supplemental information can be found online at https://doi.org/10.1016/j.celrep.2025.116592.

Received: February 4, 2025
Revised: August 22, 2025
Accepted: November 3, 2025
Published: November 23, 2025

REFERENCES

1. Cornelis, G. (2006). The type III secretion injectisome. Nat. Rev. Microbiol. *4*, 811–825.
2. Deng, W., Marshall, N.C., Rowland, J.L., McCoy, J.M., Worrall, L.J., Santos, A.S., Strynadka, N.C.J., and Finlay, B.B. (2017). Assembly, structure, function and regulation of type III secretion systems. Nat. Rev. Microbiol. *15*, 323–337.
3. Galán, J.E., and Wolf-Watz, H. (2006). Protein delivery into eukaryotic cells by type III secretion machines. Nature *444*, 567–573.
4. Wagner, S., Grin, I., Malmsheimer, S., Singh, N., Torres-Vargas, C.E., and Westerhausen, S. (2018). Bacterial type III secretion systems: A complex device for the delivery of bacterial effector proteins into eukaryotic host cells. FEMS Microbiol. Lett. *365*, fny201.
5. Kupferberg, L.L., and Higuchi, K. (1958). Role of calcium ions in the stimulation of growth of virulent strains of Pasteurella pestis. J. Bacteriol. *76*, 120–121.
6. Fowler, J.M., Wulff, C.R., Straley, S.C., Brubaker, R.R., and Robert Brubaker, C.R. (2009). Growth of calcium-blind mutants of Yersinia pestis at 37°C in permissive Ca^{2+}-deficient environments. Microbiology (Read.) *155*, 2509–2521.
7. Ben-Gurion, R., and Shafferman, A. (1981). Essential virulence determinants of different Yersinia species are carried on a common plasmid. Plasmid *5*, 183–187.
8. Ferber, D.M., and Brubaker, R.R. (1981). Plasmids in Yersinia pestis. Infect. Immun. *31*, 839–841.
9. Perry, R.D., Harmon, P.A., Bowmer, W.S., and Straley, S.C. (1986). A Low-Ca2' Response Operon Encodes the V Antigen of Yersinia pestis. Infect. Immun. *54*, 428–434.
10. Michiels, T., Wattiau, P., Brasseur, R., Ruysschaert, J.M., and Cornelis, G. (1990). Secretion of Yop proteins by yersiniae. Infect. Immun. *58*, 2840–2849.
11. Sturm, A., Heinemann, M., Arnoldini, M., Benecke, A., Ackermann, M., Benz, M., Dormann, J., and Hardt, W.D. (2011). The cost of virulence: Retarded growth of salmonella typhimurium cells expressing type iii secretion system 1. PLoS Pathog. *7*, e1002143.
12. Carter, P.B., Zahorchak, R.J., and Brubaker, R.R. (1980). Plague Virulence Antigens from Yersinia Enterocolitica. Infect. Immun. *28*, 638–640.
13. Sasakawa, C., Kamata, K., Sakai, T., Murayama, S.Y., Makino, S., and Yoshikawa, M. (1986). Molecular Alteration of the 140-Megadalton Plasmid Associated with Loss of Virulence and Congo Red Binding Activity in Shigella Flexneri. Infect. Immun. *51*, 470–475.
14. Wimmi, S., Fleck, M., Helbig, C., Brianceau, C., Langenfeld, K., Szymanski, W.G., Angelidou, G., Glatter, T., and Diepold, A. (2024). Pilotins are mobile T3SS components involved in assembly and substrate specificity of the bacterial type III secretion system. Mol. Microbiol. *121*, 304–323.
15. Milne-Davies, B., Helbig, C., Wimmi, S., Cheng, D.W.C., Paczia, N., and Diepold, A. (2019). Life After Secretion—Yersinia enterocolitica Rapidly Toggles Effector Secretion and Can Resume Cell Division in Response to Changing External Conditions. Front. Microbiol. *10*, 2128.
16. Büttner, D. (2012). Protein Export According to Schedule: Architecture, Assembly, and Regulation of Type III Secretion Systems from Plant- and Animal-Pathogenic Bacteria. Microbiol. Mol. Biol. Rev. *76*, 262–310.
17. Cornelis, G.R., Boland, A., Boyd, A.P., Geuijen, C., Iriarte, M., Neyt, C., Sory, M.P., and Stainier, I. (1998). The Virulence Plasmid of Yersinia , an Antihost Genome. Microbiol. Mol. Biol. Rev. *62*, 1315–1352.
18. Schubert, K.A., Xu, Y., Shao, F., and Auerbuch, V. (2020). The Yersinia Type III Secretion System as a Tool for Studying Cytosolic Innate Immune Surveillance. Annu. Rev. Microbiol. *74*, 221–245.
19. Volk, M., Vollmer, I., Heroven, A.K., and Dersch, P. (2020). Transcriptional and post-transcriptional regulatory mechanisms controlling type III secretion. Curr. Top. Microbiol. Immunol. *427*, 11–33.
20. Pienkoß, S., Javadi, S., Chaoprasid, P., Nolte, T., Twittenhoff, C., Dersch, P., and Narberhaus, F. (2021). The gatekeeper of Yersinia type III secretion is under RNA thermometer control. PLoS Pathog. *17*, e1009650.
21. Pettersson, J., Nordfelth, R., Dubinina, E., Bergman, T., Gustafsson, M., Magnusson, K.E., and Wolf-Watz, H. (1996). Modulation of Virulence Factor Expression by Pathogen Target Cell Contact. Science *273*, 1231–1233.

22. Yother, J., and Goguen, J.D. (1985). Isolation and characterization of Ca2+-blind mutants of Yersinia pestis. J. Bacteriol. *164*, 704–711.

23. Dewoody, R.S., Merritt, P.M., Marketon, M.M., Francis, M., and Forsberg, A. (2013). Regulation of the Yersinia type III secretion system: traffic control. Front. Cell. Infect. Microbiol. *3*, 4.

24. Cornelis, G.R. (2002). Yersinia type III secretion: send in the effectors. J. Cell Biol. *158*, 401–408.

25. Kudryashev, M., Diepold, A., Amstutz, M., Armitage, J.P., Stahlberg, H., and Cornelis, G.R. (2015). Yersinia enterocolitica type III secretion injectisomes form regularly spaced clusters, which incorporate new machines upon activation. Mol. Microbiol. *95*, 875–884.

26. Wang, H., Avican, K., Fahlgren, A., Erttmann, S.F., Nuss, A.M., Dersch, P., Fallman, M., Edgren, T., and Wolf-Watz, H. (2016). Increased plasmid copy number is essential for Yersinia T3SS function and virulence. Science *353*, 492–495.

27. Engling, P., Héchard, T., Edgren, T., Francis, M., Dersch, P., and Wang, H. (2023). Calcium-responsive plasmid copy number regulation is dependent on discrete YopD domains in Yersinia pseudotuberculosis. Plasmid *126*, 102683.

28. Woldringh, C.L. (2002). The role of co-transcriptional translation and protein translocation (transertion) in bacterial chromosome segregation. Mol. Microbiol. *45*, 17–29.

29. Kaval, K.G., Chimalapati, S., Siegel, S.D., Garcia, N., Jaishankar, J., Dalia, A.B., and Orth, K. (2023). Membrane-localized expression, production and assembly of Vibrio parahaemolyticus T3SS2 provides evidence for transertion. Nat. Commun. *14*, 1178.

30. Spahn, C., Middlemiss, S., Gómez-de-Mariscal, E., Henriques, R., Bode, H.B., Holden, S., and Heilemann, M. (2025). The nucleoid of rapidly growing Escherichia coli localizes close to the inner membrane and is organized by transcription, translation, and cell geometry. Nat. Commun. *16*, 3732.

31. Diepold, A., and Wagner, S. (2014). Assembly of the bacterial type III secretion machinery. FEMS Microbiol. Rev. *38*, 802–822.

32. Schneiders, S., Hechard, T., Edgren, T., Avican, K., Fällman, M., Fahlgren, A., and Wang, H. (2021). Spatiotemporal variations in growth rate and virulence plasmid copy number during Yersinia pseudotuberculosis infection. Infect. Immun. *89*, e00710-20.

33. Diepold, A., Amstutz, M., Abel, S., Sorg, I., Jenal, U., and Cornelis, G.R. (2010). Deciphering the assembly of the Yersinia type III secretion injectisome. EMBO J. *29*, 1928–1940.

34. Libby, E.A., Roggiani, M., and Goulian, M. (2012). Membrane protein expression triggers chromosomal locus repositioning in bacteria. Proc. Natl. Acad. Sci. USA *109*, 7445–7450.

35. Norris, V., and Madsen, M.S. (1995). Autocatalytic gene expression occurs via transertion and membrane domain formation and underlies differentiation in bacteria: a model. J. Mol. Biol. *253*, 739–748.

36. Birtalan, S.C., Phillips, R.M., and Ghosh, P. (2002). Three-dimensional secretion signals in chaperone-effector complexes of bacterial pathogens. Mol. Cell *9*, 971–980.

37. Trülzsch, K., Roggenkamp, A., Aepfelbacher, M., Wilharm, G., Ruckdeschel, K., and Heesemann, J. (2003). Analysis of chaperone-dependent Yop secretion/translocation and effector function using a mini-virulence plasmid of Yersinia enterocolitica. Int. J. Med. Microbiol. *293*, 167–177.

38. Schnitzbauer, J., Strauss, M.T., Schlichthaerle, T., Schueder, F., and Jungmann, R. (2017). Super-resolution microscopy with DNA-PAINT. Nat. Protoc. *12*, 1198–1228.

39. Endesfelder, U., Malkusch, S., Fricke, F., and Heilemann, M. (2014). A simple method to estimate the average localization precision of a single-molecule localization microscopy experiment. Histochem. Cell Biol. *141*, 629–638.

40. Spahn, C.K., Glaesmann, M., Grimm, J.B., Ayala, A.X., Lavis, L.D., and Heilemann, M. (2018). A toolbox for multiplexed super-resolution imaging of the E. coli nucleoid and membrane using novel PAINT labels. Sci. Rep. *8*, 14768.

41. Ester, M. (1996). A Density-Based Algorithm for Discovering Clusters in Large Spatial Databases with Noise. In Proceedings of the Second International Conference on Knowledge Discovery and Data Mining (KDD'96)).

42. Papagiannakis, A., Yu, Q., Govers, S.K., Lin, W.-H., Wingreen, N.S., and Jacobs-Wagner, C. (2024). DNA/polysome phase separation and cell width confinement couple nucleoid segregation to cell growth in *Escherichia coli*. eLife *14*, RP104276.

43. Schott, S., Scheuer, R., Ermoli, F., Glatter, T., Evguenieva-Hackenberg, E., and Diepold, A. (2023). A ParDE toxin-antitoxin system is responsible for the maintenance of the Yersinia virulence plasmid but not for type III secretion-associated growth inhibition. Front. Cell. Infect. Microbiol. *13*, 1166077.

44. Fukui, G.M., Ogg, J.E., Wessman, G.E., and Surgalla, M.J. (1957). Studies on relation of cultural conditions and virulence of Pasturella Pestis. J. Bacteriol. *74*, 714–717.

45. Wilharm, G., and Heider, C. (2014). Interrelationship between type three secretion system and metabolism in pathogenic bacteria. Front. Cell. Infect. Microbiol. *4*, 150.

46. Anderson, D.M., Ramamurthi, K.S., Tam, C., and Schneewind, O. (2002). YopD and LcrH regulate expression of Yersinia enterocolitica YopQ by a posttranscriptional mechanism and bind to yopQ RNA. J. Bacteriol. *184*, 1287–1295.

47. Francis, M.S., Wolf-Watz, H., and Forsberg, A. (2002). Regulation of type III secretion systems. Curr. Opin. Microbiol. *5*, 166–172.

48. Ramamurthi, K.S., and Schneewind, O. (2002). Type III Protein Secretion in Yersinia Species. Ann Rev Cell Bio *18*, 107–133.

49. Sturm, A., Heinemann, M., Arnoldini, M., Benecke, A., Ackermann, M., Benz, M., Dormann, J., and Hardt, W.D. (2011). The Cost of Virulence: Retarded Growth of Salmonella Typhimurium Cells Expressing Type III Secretion System 1. PLoS Pathog. *7*, 1002143.

50. Schmid, A., Neumayer, W., Trülzsch, K., Israel, L., Imhof, A., Roessle, M., Sauer, G., Richter, S., Lauw, S., Eylert, E., et al. (2009). Cross-talk between type three secretion system and metabolism in Yersinia. J. Biol. Chem. *284*, 12165–12177.

51. Zahorchak, R.J., Charnetzky, W.T., Little, R.V., and Robert Brubaker, A.R. (1979). Consequences of Ca^{2+} Deficiency on Macromolecular Syrnthesis and Adenylate Energy Charge in Yersinia Pestis. J. Bacteriol. *139*, 792–799.

52. Zhang, C., Datta, S., Ratcliff, W.C., and Hammer, B.K. (2024). Constitutive expression of the Type VI Secretion System carries no measurable fitness cost in Vibrio cholerae. Ecol. Evol. *14*, e11081.

53. Taillefer, B., Giraud, J.F., and Cascales, E. (2023). No fitness cost entailed by type VI secretion system synthesis, assembly, contraction, or disassembly in enteroaggregative Escherichia coli. J. Bacteriol. *205*, e0035723.

54. Kudryashev, M., Stenta, M., Schmelz, S., Amstutz, M., Wiesand, U., Castaño-Díez, D., Degiacomi, M.T., Münnich, S., Bleck, C.K., Kowal, J., et al. (2013). In situ structural analysis of the Yersinia enterocolitica injectisome. eLife *30*, e00792.

55. Schubert, K., Zhang, J., Muscolo, M.E., Braly, M., McCausland, J.W., Lam, H.N., Hug, K., Loven, M., Ruiz Solis, S., Estrada Escobar, M., et al. (2025). The polyadenylase PAPI is required for virulence plasmid maintenance in pathogenic bacteria. PLoS Pathog. *21*, e1012655.

56. Sadhir, I., and Murray, S.M. (2023). Mid-cell migration of the chromosomal terminus is coupled to origin segregation in Escherichia coli. Nat. Commun. *14*, 7489.

57. Wimmi, S., Balinovic, A., Brianceau, C., Pintor, K., Vielhauer, J., Turkowyd, B., Helbig, C., Fleck, M., Langenfeld, K., Kahnt, J., et al. (2024). Cytosolic sorting platform complexes shuttle type III secretion system effectors to the injectisome in Yersinia enterocolitica. Nat. Microbiol. *9*, 185–199.

58. Stebbins, C.E., and Galán, J.E. (2001). Maintenance of an unfolded polypeptide by a cognate chaperone in bacterial type III secretion. Nature *414*, 77–81.

59. Nevo-Dinur, K., Nussbaum-Shochat, A., Ben-Yehuda, S., and Amster-Choder, O. (2011). Translation-independent localization of mRNA in E. coli. Science *331*, 1081–1084.

60. Mondal, J., Bratton, B.P., Li, Y., Yethiraj, A., and Weisshaar, J.C. (2011). Entropy-based mechanism of ribosome-nucleoid segregation in E. coli Cells. Biophys. J. *100*, 2605–2613.

61. Stracy, M., Lesterlin, C., Garza de Leon, F., Uphoff, S., Zawadzki, P., and Kapanidis, A.N. (2015). Live-cell superresolution microscopy reveals the organization of RNA polymerase in the bacterial nucleoid. Proc. Natl. Acad. Sci. USA *112*, E4390–E4399.

62. Ladouceur, A.M., Parmar, B.S., Biedzinski, S., Wall, J., Tope, S.G., Cohn, D., Kim, A., Soubry, N., Reyes-Lamothe, R., and Weber, S.C. (2020). Clusters of bacterial RNA polymerase are biomolecular condensates that assemble through liquid-liquid phase separation. Proc. Natl. Acad. Sci. USA *117*, 18540–18549.

63. Martin, C.M., Sun, Z., Zhou, Y.N., and Jin, D.J. (2018). Extrachromosomal nucleolus-like compartmentalization by a plasmid-borne ribosomal RNA operon and its role in nucleoid compaction. Front. Microbiol. *9*, 354211.

64. Cornet, F., Blanchais, C., Dusfour-Castan, R., Meunier, A., Quebre, V., Sekkouri Alaoui, H., Boudsoq, F., Campos, M., Crozat, E., Guynet, C., et al. (2023). DNA Segregation in Enterobacteria. EcoSal Plus *11*, eesp00382020.

65. Hu, L., Rech, J., Bouet, J.Y., and Liu, J. (2021). Spatial control over near-critical-point operation ensures fidelity of ParABS-mediated DNA partition. Biophys. J. *120*, 3911–3924.

66. Qian, J., Cartee, A., Xu, W., Yan, Y., Wang, B., Artsimovitch, I., Dunlap, D., and Finzi, L. (2024). Reciprocating RNA Polymerase batters through roadblocks. Nat. Commun. *15*, 3193.

67. Papagiannakis, A., Yu, Q., Govers, S.K., Lin, W.H., Wingreen, N.S., and Jacobs-Wagner, C. (2025). Nonequilibrium polysome dynamics promote chromosome segregation and its coupling to cell growth in Escherichia coli. eLife *14*, RP104276.

68. Meyer, I., Volk, M., Salto, I., Moesser, T., Chaoprasid, P., Herbrüggen, A.S., Rohde, M., Beckstette, M., Heroven, A.K., and Dersch, P. (2024). RNase-mediated reprogramming of Yersinia virulence. PLoS Pathog. *20*, e1011965.

69. Wu, F., Swain, P., Kuijpers, L., Zheng, X., Felter, K., Guurink, M., Solari, J., Jun, S., Shimizu, T.S., Chaudhuri, D., et al. (2019). Cell Boundary Confinement Sets the Size and Position of the E. coli Chromosome. Curr. Biol. *29*, 2131–2144.e4.

70. Schumacher, M.A., and Zeng, W. (2016). Structures of the nucleoid occlusion protein SlmA bound to DNA and the C-terminal domain of the cytoskeletal protein FtsZ. Proc. Natl. Acad. Sci. USA *113*, 4988–4993.

71. Adams, D.W., Wu, L.J., and Errington, J. (2014). Cell cycle regulation by the bacterial nucleoid. Curr. Opin. Microbiol. *22*, 94–101.

72. Dewachter, L., Verstraeten, N., Fauvart, M., and Michiels, J. (2018). An integrative view of cell cycle control in Escherichia coli. FEMS Microbiol. Rev. *42*, 116–136.

73. Jensen, R.B., and Shapiro, L. (1999). Chromosome segregation during the prokaryotic cell division cycle. Curr. Opin. Cell Biol. *11*, 726–731.

74. Böhme, K., Steinmann, R., Kortmann, J., Seekircher, S., Heroven, A.K., Berger, E., Pisano, F., Thiermann, T., Wolf-Watz, H., Narberhaus, F., and Dersch, P. (2012). Concerted Actions of a Thermo-labile Regulator and a Unique Intergenic RNA Thermosensor Control Yersinia Virulence. PLoS Pathog. *8*, 1002518.

75. Erhardt, M., and Dersch, P. (2015). Regulatory principles governing Salmonella and Yersinia virulence. Front. Microbiol. *6*, 949.

76. Kaniga, K., Delor, I., and Cornelis, G.R. (1991). A Wide-Host-Range Suicide Vector for Improving Reverse Genetics in Gram-Negative Bacteria: Inactivation of the BlaA Gene of Yersinia Enterocolitica. Gene *109*, 137–141.

77. Sory, M.-P., Boland, A., Lambermont, I., and Cornelis, G.R. (1995). Identification of the YopE and YopH Domains Required for Secretion and Internalization into the Cytosol of Macrophages, Using the CyaA Gene Fusion Approach. Proc. Natl. Acad. Sci. USA *92*, 11998–12002.

78. Boland, A., Sory, M.-P., Iriarte, M., Kerbourch, C., Wattiau, P., and Cornelis, G.R. (1996). Status of YopM and YopN in the Yersinia Yop Virulon: YopM of Yenterocolitica Is Internalized inside the Cytosol of PU5-1.8 Macrophages by the YopB, D, N Delivery Apparatus. EMBO J. *15*, 5191–5201.

79. Spahn, C., Diepold, A., and Ermoli, F. (2024). StarDist model and data for the segmentation of Yersinia enterocolitica cells in widefield images. Zenodo. https://doi.org/10.5281/ZENODO.11105050.

80. Schindelin, J., Arganda-Carreras, I., Frise, E., Kaynig, V., Longair, M., Pietzsch, T., Preibisch, S., Rueden, C., Saalfeld, S., Schmid, B., et al. (2012). Fiji: an open-source platform for biological-image analysis. Nat. Methods *9*, 676–682.

81. Hartmann, R., F van Teeseling, M.C., Thanbichler, M., Drescher, K., and Knut, D.,C. (2020). BacStalk: A comprehensive and interactive image analysis software tool for bacterial cell biology. Mol. Microbiol. *114*, 140–150.

82. Schmidt, U., Weigert, M., Broaddus, C., and Myers, G. (2018). Cell detection with star-convex polygons. In Lecture Notes in Computer Science, *11071* (LNCS), pp. 265–273.

83. Paintdakhi, A., Parry, B., Campos, M., Irnov, I., Elf, J., Surovtsev, I., and Jacobs-Wagner, C. (2015). Oufti: an integrated software package for high-accuracy, high-throughput quantitative microscopy analysis. Mol. Microbiol. *99*, 767–777.

84. Spahn, C., Gómez-de-Mariscal, E., Laine, R.F., Pereira, P.M., von Chamier, L., Conduit, M., Pinho, M.G., Jacquemet, G., Holden, S., Heilemann, M., and Henriques, R. (2022). DeepBacs for multi-task bacterial image analysis using open-source deep learning approaches. Commun. Biol. *5*, 688.

85. Skinner, S.O., Sepúlveda, L.A., Xu, H., and Golding, I. (2013). Measuring mRNA copy-number in individual Escherichia coli cells using single-molecule fluorescent in situ hybridization (smFISH). Nat. Protoc. *8*, 1100.

86. Strauss, M.T. (2022). Picasso-server: a community-based, open-source processing framework for super-resolution data. Commun. Biol. *5*, 930–933.

87. Schmittgen, T.D., and Livak, K.J. (2008). Analyzing real-time PCR data by the comparative CT method. Nat. Protoc. *3*, 1101–1108.

STAR★METHODS

KEY RESOURCES TABLE

REAGENT or RESOURCE	SOURCE	IDENTIFIER
Antibodies		
Rabbit polyclonal anti-mCherry	BioVision	Cat#5993; RRID: AB_1975001
Goat polyclonal anti-rabbit-IgG, HRP-coupled	Sigma-Aldrich	Cat#A8275; RRID: AB_258382
Bacterial strains and plasmids		
All strains and plasmids used in this study are listed in Tables S2 and S3.	This paper; Sadhir et al.[56]; Kaniga et al.[76]; Sory et al.[77]; Kudryashev et al.[54]; Boland et al.[33,78]; Diepold et al.[33]; and Wimmi et al.[57]	See Tables S2 and S3
Critical commercial assays		
PureLink Miniprep Kit	Thermofisher Scientific	#K210010
Luna Universal qPCR MasterMix	New England Biolabs	#M3003L
Deposited data		
Model used for the segmentation of individual *Y. enterocolitica* cells for data analysis and demograph generation	This paper[79]	Zenodo within the DeepBacs repository, accession code: 11105050
Chemicals, peptides, and recombinant proteins		
E. coli tRNA	Sigma-Aldrich	Cat# R1750-500UN
Dextrane sulfate sodium salt	Sigma-Aldrich	Cat# D8906-10G
Formamide, deionized	VWR	Cat# 0606-500mL
Vanadyl ribonucleoside complex	New England Biolabs	Cat# S1402S
BSA (nuclease-free)	Carl Roth	Cat# 3737.2
PBS (nuclease-free)	ThermoFisher Scientific	Cat# AM9625
Ultrapure 1M Tris pH 8.0	ThermoFisher Scientific	Cat# 15568025
20x SSC (nuclease-free)	ThermoFisher Scientific	Cat# AM9770
0.1% Poly-L-Lysine	Sigma-Aldrich	Cat# P8920
90 nm Gold NanoUrchins	Cytodiagnostics	Cat# GU-90-20
Low-melting agarose	Sigma-Aldrich	Cat# A4018
Formaldehyde	Sigma-Aldrich	Cat# 252549
Oligonucleotides		
All oligonucleotides, including the specific FISH probes used in this study are listed in Table S4	Microsynth SeqLab	See Table S4
Cy5-labeled EUB338 probe GCTGCCTCCCGTAGGAGTTTATACATCTA	Sigma-Aldrich	N/A
P1 imager strand TAGATGTAT-ATTO655	metabion	N/A
Software and algorithms		
Fiji	Schindelin et al.[80]	https://fiji.sc/
Origin 2023b	OriginLab	N/A
MATLAB R2020a	Mathworks	N/A
BacStalk	Hartmann et al.[81]	https://drescherlab.org/data/bacstalk/
StarDist	Schmidt et al.[82]	https://github.com/jungmannlab/picasso
Oufti	Paintdakhi et al.[83]	https://oufti.org/
Picasso v.0.7.0 and v.0.8.2	Schnitzbauer et al.[38]	https://github.com/jungmannlab/picasso

EXPERIMENTAL MODEL AND STUDY PARTICIPANT DETAILS

The *Y. enterocolitica* strains used in this study are based on the *Y. enterocolitica* wild-type strain MRS40.

METHOD DETAILS

Bacterial strain generation and genetic constructs

All *Y. enterocolitica* fusion proteins used in this study are expressed as endogenous fusions from their native location on the pYV virulence plasmid; the genes were introduced by allelic exchange.[76] Likewise, the $parS_{P1}$ sequence was integrated on the pYV plasmid by allelic exchange; the C-terminal part of *yopE*, encoding for amino acids 139–219 of the enzymatic GTPase-activating protein domain was replaced by a short linker domain (peptide sequence GGSGGSGGRSR), followed by a stop codon and the $parS_{P1}$ sequence (Figure S1). Completion of the allelic exchange was tested for by plating diploid bacteria on plates containing 5% sucrose and gene-specific PCR. A list of strains and plasmids used in this study can be found in Tables S2 and S3.

Bacterial cultivation, secretion assay, and protein detection

Y. enterocolitica overnight cultures were grown on a shaking incubator at 28°C in brain heart infusion medium (BHI) supplemented with nalidixic acid (Nal, 35 μg/mL). Day cultures (BHI supplemented with 35 μg/mL Nal, 20 mM $MgCl_2$, 0.4% glycerol, and 5 mM EGTA for secreting conditions or 5 mM $CaCl_2$ for non-secreting conditions) were inoculated from stationary overnight cultures to an OD_{600} of 0.1 by directly adding the required amount of the overnight culture to fresh medium. To select for expression plasmid maintenance, 200 μg/mL ampicillin was added, where required. Day cultures were incubated at 28°C for 90 min after the inoculum. Expression of the *yop* regulon was then induced by a rapid temperature shift to 37°C. Where needed, protein expression from the pFHCP1-mScarlet-$ParB_{P1}$ plasmid was induced at the temperature shift by adding 100 μM Isopropyl β-D-1-thiogalactopyranoside (IPTG), as described for the respective experiments. Unless specified otherwise, bacteria were incubated for 150 min after the shift to 37°C. For the observation of pYV and overall DNA localization over time after induction of secretion (Figure 5), bacteria were first incubated under non-secreting conditions for 150 min at 37°C and harvested by centrifugation (2400 *g*, 4 min). Secretion was then induced by careful resuspension in pre-warmed secreting medium at 37° (t = 0). For dilution plating at these time points, 50 μL of culture consecutively 1:50 diluted for three times (20μl + 980 μL ice-cold medium) were plated on LB-agar plates containing 35 μg/mL Nal. For secretion assays, 2 mL of the culture supernatant was harvested by centrifugation (10 min, 21,000 *g*) 180 min after the shift to 37°C. Proteins in the supernatant were precipitated with 10% trichloroacetic acid (TCA) at 4°C for 1–8 h. Precipitated proteins were collected by centrifugation (15 min, 21,000 *g*, 4°C). After washing with ice-cold acetone (1 mL), the pellets were resuspended in SDS-PAGE loading buffer and normalized to 0.3 OD units (ODu)/15 μL for total cell analysis, or 0.6 ODu/15 μL for secretion assays (1 ODu = 1 mL of culture at OD_{600} of 1, ~5 x 10^8 *Y. enterocolitica*). After resuspension, samples were incubated for 5 min at 99°C and 15 μL were applied to SDS-PAGE analysis. Protein separation was performed on 15% SDS-PAGE gels and protein sizes were determined using the BlueClassic Prestained Marker (Jena Biosciences) as standard. For visualization, the gels were stained with FastGene-Q-stain (NipponGenetics). For immunoblots, the separated proteins were transferred to a nitrocellulose membrane. Primary rabbit anti-mCherry antibody (BioVision 5993, 1:2,000) was used in combination with a secondary anti-rabbit antibody conjugated to horseradish peroxidase (Sigma-Aldrich A8275, 1:10,000). For visualization, Immobilon Forte chemiluminescence substrate (Sigma-Aldrich) was used in a LAS-4000 Luminescence Image Analyzer.

Fluorescence microscopy

For fluorescence microscopy, bacteria were grown as described above. After 150 min at 37°C, 500 μL of culture were harvested by centrifugation (2 min, 2400 *g*) and resuspended in 250 μL of microscopy medium (100 mM 2-[4-(2-Hydroxyethyl)piperazin-1-yl]ethane-1-sulfonic acid (HEPES) pH 7.2, 5 mM $(NH_4)_2SO_4$, 100 mM NaCl, 20 mM sodium glutamate, 10 mM $MgCl_2$, 5 mM K_2SO_4, 50 mM 2-(N-morpholino) ethane sulfonic acid (MES), 50 mM glycine). 2 μL of bacterial resuspension were spotted on an agarose pad (1.5% low melting agarose (Sigma-Aldrich) in microscopy medium, 1% casamino acids, 5 mM EGTA) in a glass depression slide (Marienfeld). For imaging, a Deltavision Elite Optical Sectioning Microscope equipped with a UPlanSApo 100×/1.40 oil objective (Olympus) and an EDGE sCMOS_5.5 camera (Photometrics) was used. z stacks with 9 slices (Δz = 0.15 μm) were acquired. The mScarlet signal was visualized using a mCherry filter set (excitation: 575/25 nm, emission: 625/45 nm) with 0.2 s exposure time. Images were processed with FIJI (ImageJ 1.51f/1.52i/1.52n).[80] Fluorescence quantification was performed in FIJI. For visualization purposes, selected fields of view adjusted identically for brightness and contrast within the compared image sets are shown.

For DNA staining, after 150 min at 37°C, 1 mL of cells were harvested and resuspended in 50 μL fresh minimal medium supplemented with 1 μg/mL DAPI. After 3 min incubation at 37°C in the dark, cells were pelleted and resuspended in 100 μL and imaged as previously described. The DAPI signal was visualized using the DAPI filter set (excitation: 390/18 nm, emission: 435/48 nm) with 0.2 s exposure time. For data analysis and demograph generation, individual *Y. enterocolitica* cells were first segmented using the neural network StarDist.[82] The model is deposited on Zenodo within the DeepBacs[84] repository under the accession code 11105050.[79] Segmented cells were loaded into BacStalk[81] for cell length, width, area, and DAPI signal quantification. Single-cell maximal DNA intensity was represented according to cell length.

Quantification and localization of fluorescent pYV foci

To quantify the number of pYV spots, a mScarlet-I fused $ParB_{P1}$ (mScarlet-I-$ParB_{P1}$) cloned under an IPTG-inducible promoter was expressed from plasmid in a strain harboring the correspondent *parSP1* sequence in the pYV plasmid ($YopE_{1-138}$-$parS_{P1}$). For fluorescent spot visualization, *Y. enterocolitica* cells were first segmented using the neural network StarDist.[82] Spot detection and

localization were performed on segmented cells in Oufti[83] with the following spot detection parameters optimized for the dataset. Data were then analyzed in MATLAB (MATLAB R2020a) and the spot localization was displayed as distance from the centerline (d in pixels, pixel size = (64.8 nm)[2]). To determine the localization of foci along the longitudinal axis, fluorescent foci, the cell center, and cell poles were manually classified in a set of images for which the conditions were blinded, and the relative location was determined as the ratio of the distances of cell center to spot and cell center to respective cell pole. As secretion influences the length of bacteria, we determined the relative localization of pYV plasmids on the midcell to cell pole line (0 = central localization, 1 = polar localization).

mRNA fluorescence *in situ* hybridization

Cells were grown for mRNA Fluorescence *in situ* hybridization (FISH), as previously described. After 150 min at 37°C, cells were prepared according to.[85] 3 x 10^9 cells were fixed directly by adding formaldehyde (3.7% v/w) and incubated for 30 min, gently mixing. The cell pellet was washed twice with 1 mL PBS (3.5 min, 600 *g*) and then resuspended for permeabilization in 70% ethanol and incubated while mixing gently. After 1 h, the cell pellet was resuspended in 1 mL washing solution (formamide 40% v/w, saline sodium citrate (SSC) buffer 2x) and mixed for 5 min. Cells were pelleted (7 min, 600 *g*) and resuspended in 50 μL hybridization solution (in 10 mL, 1 g dextran sulfate, 3.530 μL formamide, 10 mg *E.coli* tRNA, 1 mL 20x SSC, 200 mM vanadyl ribonucleoside complex (VRC) and 50 mg/mL BSA) mixed with the probe solution (1 μM final concentration). Samples were incubated O/N at 30°C. After O/N hybridization with the probes, 10 μL of the sample was washed two times with 200 μL of wash solution, with a 30 min incubation at 30°C with the solution before the second centrifugation. The washing steps are repeated two times to ensure the removal of any probe traces. For sample immobilization and preparation for imaging 10 μL of the hybridization mixture were washed thrice with washing buffer (2x SSC, 40% formamide) for 30 min at 30°C. All steps were performed with RNase-free solutions and in RNase-free environment. Cells were finally resuspended in 150 μL RNase-free PBS and immobilized on KOH-cleaned (3 M, 1 h) and PLL-coated chamber slides. Chambers were washed twice with RNase-free PBS to remove non-adherent cells. Fiducial markers (90 nm gold nano-urchins, Cytodiagnostics) were added and allowed to settle for 30 min, before washing and blocking the cells with 2% RNase-free BSA (Carl Roth 3737.2) for 30 min. Finally, cells were washed with RNase-free PBS twice and stored at 4°C or imaged.

Single-molecule imaging

All single-molecule imaging experiments were performed on a commercial N-STORM system (Nikon Instruments) equipped with a 100x Apo TIRF oil objective (NA 1.49) and an Andor iXon Ultra 897 EMCCD camera. For DNA-PAINT imaging, 0.5–5 nM P1-ATTO655 imager strand in imaging buffer (100 mM Tris pH 8.0 + 500 mM NaCl) was added to the samples. Samples were imaged in HILO mode using 1 kW/cm^2 640 nm illumination, an exposure time of 150 ms, a readout rate of 1 MHz, a preamplifier of 1 and an EM gain of 50. 30,000 frames were acquired for sr-smRNA-FISH imaging. Conventional PAINT imaging of DNA and membrane was performed using JF_{646}-Hoechst (200–400 pM) and Nile Red (200–400 pM) in DNA-PAINT imaging buffer to maintain osmolality and prevent cell shrinkage. In contrast to DNA-PAINT imaging, the EM-gain was increased to 200–400, using a readout rate of 10 MHz. 3D DNA-PAINT images were acquired as described with the difference of using an astigmatic lens in the emission pathway. For reconstruction, we recorded a 3D calibration measurement on surface-immobilized fluorescent microsphere beads (Tetraspecks, 100 nm diameter, Thermo Fisher Scientific). 3D fitting was performed with Picasso and resulting localization files were post-processed as described below.

SMLM images were analyzed using Picasso.[86] Drift correction was performed using RCC with a window size of 500–1000 frames. Subsequent frame localizations were linked using a radius of 1 px and allowing for 1 dark frame. PSF width σ in x and y was filtered according to 64 nm < $\sigma_{x/y}$ < 208 nm (Nile Red) or 80 nm < $\sigma_{x/y}$ < 224 nm (ATTO655 and JF_{646}-Hoechst). Images were registered in Fiji using cell boundaries extracted from the Nile Red image.

Counting of mRNA clusters

The number of mRNA clusters in individual cells were determined using the DBSCAN algorithm implemented in the Picasso software. DBSCAN analysis requires two parameters, namely the search radius ε and the minimum number of molecules in the search radius required for the localization to be attributed to a cluster (minpts). We set ε to twice the value of the experimental localization precision (determined via NeNA analysis, 10.6 nm). minpts was determined by manually picking 200–300 apparent mRNA clusters (see Figure 3A, green circles) and calculating the median value of localizations contained in each picked region. Of note, we performed this analysis on localization files not corrected for subsequent-frame localizations (linking). The reason for this is that true DNA-PAINT signals have a longer binding time than the unspecific binding of imager strands, leading to multiple localizations and an improved signal-to-background ratio in the reconstructed image. To remove clusters that origin from single, very long binding events (which result in clusters with many localizations), we filtered the DBSCAN-derived clusters by the standard deviation of the frame number (frame s.d.). If all localizations occur in a small time window, the frame s.d. is low, while recurring binding events over the entire acquisition period lead to a high frame s.d. We determined a cutoff value of 5,000 frames for the frame s.d. based on the negative control (secreting conditions, no FISH probes added during sample preparation). Finally, we rendered an image in which each true cluster adds 1 gray value to the pixel coordinates of its centroid. Finally, the number of clusters were determined by measuring the intensity within the cell outlines. Key steps of the pipeline are shown in Figure S5. Statistical analysis of cluster numbers and densities was performed with Origin 2023b (OriginLab).

Measurement of intensity profiles in super-resolved population average images

Population averages were generated based on a strategy published for diffraction-limited images.[30] Individual cells were isolated from multicolor super-resolution images and normalized for cell length and width based on the Potomac Gold membrane channel. Individual channels were then averaged using the "Z-Project" plugin in Fiji and recombining the channels resulted in the final population average images. Line profiles were measured along the bacterial long axis using a line width corresponding to 80% of the normalized cell width.

qPCR

Total genomic DNA of *Y. enterocolitica* cells grown as described above (2 x 10^9 cells) was extracted using the PureLink Miniprep Kit (Thermofisher Scientific) according to the manufacturer's protocol. qPCR reactions were performed on an Applied Biosystems 7500 Real-Time PCR system using the Luna Universal qPCR MasterMix (New England Biolabs) and the primers listed in Table S4. Data analysis was performed using the comparative threshold cycle (C_T) method.[87]

QUANTIFICATION AND STATISTICAL ANALYSIS

Quantitative data are displayed as the mean, displayed by boxes or black bars, and individual data points, indicated by spots or circles, from the number of biological replicates that is stated in the figure legends. In Figure 1, dotted lines represent median and quartiles. In Figure 4A, the standard deviation is indicated by whiskers. Statistical analysis was performed using a non-parametric *t* test, unless indicated otherwise in the respective figure legends, with the statistical significance represented by asterisks, ns, $p > 0.05$; *, $p < 0.05$; **, $p < 0.01$; ***, $p < 0.001$; ****, $p < 0.0001$.